Progress in PHOTOVOLTAICS

PROGRESS IN PHOTOVOLTAICS: RESEARCH AND APPLICATIONS
Prog. Photovolt: Res. Appl. 2016; **24**:760–773
Published online 18 December 2015 in Wiley Online Library (wileyonlinelibrary.com). DOI: 10.1002/pip.2722

RESEARCH ARTICLE

Determination of subcell I–V characteristics of multijunction solar cells using optical coupling

Helmut Nesswetter[1,2], Norman R. Jost[1,3], Paolo Lugli[2], Andreas W. Bett[4] and Claus G. Zimmermann[1]*

[1] Solar Array Center, Airbus Defence & Space, 81663 Munich, Germany
[2] Institute for Nanoelectronics, Technical University of Munich, Arcisstr. 21, 80333 Munich, Germany
[3] Institute of Physics, Technical University of Freiberg, Akademiestr. 6, 09596 Freiberg, Germany
[4] Fraunhofer Institute for Solar Energy Systems ISE, Heidenhofstr. 2, 79110 Freiburg, Germany

ABSTRACT

A method for the determination of the subcell I–V characteristics of multijunction solar cells in the presence of optical coupling is presented and applied to a $Ga_{0.50}In_{0.50}P/Ga_{0.99}In_{0.01}As/Ge$ triple-junction solar cell. Each of the subcells is described by a two-diode model and can be illuminated by a narrowband light source externally. Optical coupling is then used explicitly to generate current in one subcell, which is not illuminated externally. This approach yields the magnitude of optical coupling and a relationship between the two diode parameters of each subcell. The remaining cell parameters are determined with the help of pulsed illumination. In this fashion, the open circuit voltage of individual subcells is accessible, despite the fact that not all junctions are illuminated. Copyright © 2015 John Wiley & Sons, Ltd.

KEYWORDS

optical coupling; multijunction solar cell; characterization; subcell diode parameters

***Correspondence**

Claus Zimmermann, Airbus DS, Munich, Germany.
E-mail: claus.zimmermann@airbus.com

Received 3 May 2015; Revised 13 September 2015; Accepted 27 October 2015

1. INTRODUCTION

Today's most efficient solar cells are based on multijunction concepts that are better adjusted to the sun spectrum than single-junction solar cells [1]. Triple-junction solar cells composed of III–V semiconductors are used in terrestrial concentrator systems and space applications [2]. But also amorphous and microcrystalline silicon [3] and organic multijunction solar cells [4] are under investigation. Common to all of them is a two-terminal device structure that is complicating the characterization and consequently the optimization of the individual subcells. The subcell photocurrent can be assessed with the help of the external quantum efficiency (EQE), which is measured under bias light and bias voltage [5]. Especially III–V solar cells with a high ratio of radiative to non-radiative recombination can as well be analyzed by electro- and photoluminescence (PL) [6,7]. The subcell open circuit voltages can be determined with combined electroluminescence and EQE measurements [8] or voltage-dependent capacitance analysis [9].

To extract the complete subcell I–V curves is considerably more difficult. In dark and illuminated I–V curve measurements, the measured voltage is the sum of all subcell voltages. The subcell that generates the lowest photocurrent under the illumination spectrum limits the short circuit current in the absence of shunting. Using different spectra and therefore different limitation conditions together with EQE measurements and theoretical considerations is a possibility to extract the I–V characteristics of the individual subcells [10–12]. The subcell I–V curves can also be determined by a modified suns-V_{oc} method [13] and by combined EQE and electroluminescence measurements [14].

Next to the electrical coupling of the subcells, there is also optical coupling that is affecting the combined I–V curve of the cell, an effect that has not been taken into account in the work summarized previously. A photon emitted as a result of radiative recombination in one subcell can be absorbed in the subcell with lower bandgap underneath [15–17]. This effect is typically investigated in the context of EQE measurements [18,19]. With constantly improving

material quality, optical coupling becomes more and more important, and thus, its theoretical and experimental influence on the parameters and efficiency of multijunction solar cells has been investigated in detail recently [20–23]. Specifically, Steiner and Geisz [20] determined the ratio of the two dark saturation currents I_{01} and I_{02} of each subcell as well as the optical coupling parameters by measuring the photocurrents of the individual subcells under different illumination conditions. We recently proposed a special pulsed suns-V_{oc} method that uses the optical coupling effect as light source for the non-externally illuminated subcell. Together with an approach to measure the open circuit voltage of the illuminated subcells via pulsed illumination, I_{01} and I_{02} of each subcell can be determined in absolute terms [24].

Anyhow, in both approaches, the magnitude of the optical coupling has to be determined [20], which requires the knowledge of the subcell photocurrents. Assuming ideal I–V curves, the short circuit current of the cell under different biasing conditions is directly related to the photocurrent of the limiting subcell. It is the purpose of this paper to suggest an adapted method that is able to deal with non-ideal I–V curves, which exhibit shunt resistance and more importantly, a non-ideal reverse characteristic. Although these non-idealities are themselves not quantified, I_{01} and I_{02} are extracted accurately by choosing the correct measurement conditions. With this focus, optical coupling is introduced in this work as current source, depending on the biasing voltage of the exciting subcell and not as a current source depending on the available recombination current [20].

2. EXPERIMENT

The I–V characteristic of a pn-junction solar cell is described by a two-diode model [25]:

$$I = I_{ph} - I_{01}\left(e^{\frac{qV}{kT}} - 1\right) - I_{02}\left(e^{\frac{qV}{2kT}} - 1\right) \tag{1}$$

where I_{01} and I_{02} are the dark saturation currents for the neutral respectively depletion region and I, V, q, k, and T have their usual meaning. The photocurrent under illumination I_{ph} is added according to the superposition principle [26]. In this simplified two-diode model, series and shunt resistances are neglected. For a multijunction solar cell composed of different semiconductor materials, each subcell can be described by Eq. (1) with individual parameters. The tunneling junctions between the subcells have a negligible influence on the I–V curve of multijunction solar cells for low-level injection and non-concentrated sunlight and are not considered in the following [27].

Under illumination and a given biasing voltage V, there is radiative recombination whose spectral distribution $\varphi(E)$ is given by the advanced reciprocity relation for electroluminescence and PL [28]:

$$\varphi(E) = \varphi_{sc}(E) + EQE(E)\varphi_{BB}(E)\left(e^{\frac{qV}{kT}} - 1\right) \tag{2}$$

E denotes the photon energy, $\varphi_{sc}(E)$ the luminescence at short circuit conditions, and $\varphi_{BB}(E)$ the radiation of a black body at cell temperature T. For high-quality cells, $\varphi_{sc}(E)$ can be neglected,[1] and this simplification is applied in the following. A fraction x of the photons emitted, for example, downwards from the top cell towards the middle cell, will be reabsorbed in the middle cell. This fraction is determined by merely geometric aspects and the refractive index of the individual semiconductor layers. It is assumed to be independent on the level of injection and generates an additional optical coupling photocurrent $I_{oc,mid}$ there:

$$I_{oc,mid} = x\int IQE_{mid}(E)\varphi_{top}(E)dE \tag{3}$$

$IQE_{mid}(E)$ denotes the internal quantum efficiency of the middle cell. With defining

$$C_{tm} := x\int EQE_{top}(E)IQE_{mid}(E)\varphi_{BB}(E)dE \tag{4}$$

and using Eq.(2), Eq. (3) can be written as

$$I_{oc,mid} = C_{tm}\left(e^{\frac{qV_{top}}{kT}} - 1\right) \tag{5}$$

By defining a constant η_{tm} as

$$\eta_{tm} = C_{tm}/I_{01,top} \tag{6}$$

Eq. (5) becomes

$$I_{oc,mid} = \eta_{tm}I_{01,top}\left(e^{\frac{qV_{top}}{kT}} - 1\right) \tag{7}$$

This is the typical definition [20] of the coupling efficiency η_{tm} as proportionality constant between the current through the first diode and the optical coupling current $I_{oc,mid}$.

An upper limit for the optical coupling current $I_{oc,mid}$ can be found by assuming an ideal diode characteristic with only radiative recombination in the top cell [29]. In this case, Eq. (1) becomes

$$I_{top} = I_{ph,top} - \int EQE_{top}(E)\varphi_{BB}(E)dE\left(e^{\frac{qV_{top}}{kT}} - 1\right) \tag{8}$$

With the help of Eqns (4), (5), and (8) and applying open circuit conditions for the top cell, an upper limit for the ratio of $I_{oc,mid}$ to $I_{ph,top}$ is obtained:

[1] With the help of representative component cells, it was verified that the ratio of the short circuit luminescence to the open circuit luminescence is below 3% for the top cell and below 1% for the middle cell.

$$\frac{I_{oc,mid}}{I_{ph,top}} < \frac{x\int EQE_{top}(E)IQE_{mid}(E)\varphi_{BB}(E)dE}{\int EQE_{top}(E)\varphi_{BB}(E)dE} \quad (9)$$

For any efficient multijunction cell, quantum efficiencies are close to one, and moreover, the IQE of the middle cell extends all the way through the range of spectral sensitivity of the top cell. Thus, based on Eq. (9), it can be concluded that $I_{oc,mid}/I_{ph,top} < x$. The refractive indices of the materials used in the stack can be chosen that the fraction x can approach 1 [21], and thus, in ideal materials the optical coupling current could approach the photocurrent of the exciting subcell under open circuit conditions. For the cell analyzed in this work, the ratio of the two current ratios is lower, that is, $I_{oc,mid}/I_{ph,top} \approx 0.01$ and $I_{oc,bot}/I_{ph,mid} \approx 0.29$. This is not only because of the non-ideal material quality but also because of the measurement of this ratio under short circuit conditions.

In the presence of optical coupling, the equivalent circuit of a multijunction solar cell has to be modified by additional current sources that are exponentially dependent on the voltage drop over the pn-junction of the subcell shown previously. Figure 1 shows the equivalent circuit for a triple-junction solar cell based on these prerequisites.

Especially for illumination conditions with monochromatic light sources, the effect of optical coupling is clearly visible in a subcell that is not excited externally. In general, the overall current of a multijunction cell for voltages V_{ext} smaller than the open circuit voltage $V_{oc,MJ}$ of the entire cell is mainly influenced by the photocurrent and the reverse characteristic of the limiting subcell. This implies that for well-behaving cells, which have no strong shunts or high reverse currents, only this photocurrent is dominating the I–V curve for $V_{ext} < V_{oc,MJ}$.

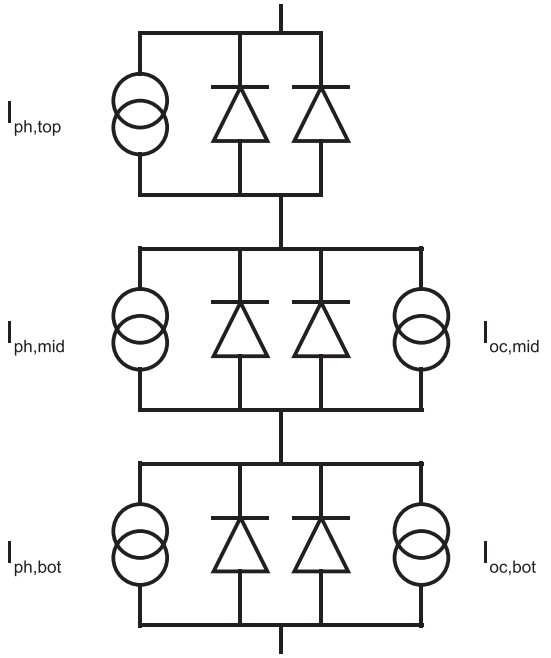

Figure 1. Equivalent circuit of a triple-junction solar cell based on the simplified two-diode model with individual current sources for external illumination on the left and additional current sources due to optical coupling in the middle and bottom subcells on the right.

Thus, the voltage-dependent optical coupling current is mainly determining the external multijunction current, if one subcell is not illuminated externally. As the optical coupling current is significantly lower than the photocurrent in the exciting subcell, as shown earlier, this exciting subcell is close to its individual open circuit voltage for $V_{ext} < V_{oc,MJ}$. Consequently, the exciting subcell is in the steep part of its I–V curve, and a small change in external multijunction current does not change its voltage [12]. As the voltage of the exciting subcell, which is responsible for the optical coupling, is stable, the optical coupling current is constant, and the I–V curve is flat for this external voltage range.

To illuminate the three subcells independently, the electroluminescence and PL setup described in Reference [7] was used. The top cell is illuminated by a 405-nm LED array, whose radiation is completely absorbed there. An 803-nm and a 975-nm diode lasers are used for the external illumination of middle and bottom cells. Again, photons of this wavelength are solely absorbed in the middle and bottom cells, respectively. The I–V curves were acquired at 300 K with a source–measure unit and four-wire connections. All measurements were performed on a 30.2 cm^2 $Ga_{0.50}In_{0.50}P/Ga_{0.99}In_{0.01}As/Ge$ triple-junction solar cell designed for space applications. Details of the approximate layer stacking of a similar solar cell can be found in Reference [30].

Typical I–V characteristics measured under various illumination conditions are shown in Figure 2 on a logarithmic scale. To deal with negative current values, the absolute value of the current is shown in the logarithmic plot. The legend indicates which subcells are illuminated externally. The intensity of the individual light sources was chosen to result in photocurrents of 0.475 A for the top subcell, 0.500 A for the middle subcell, and 1.342 A for the bottom subcell. Because the exact values are not crucial for the qualitative discussion in the following, the determination of these photocurrents will be explained in more detail in Section 3. For the black I–V curve (squared symbols), all three subcells are externally illuminated. For all the other depicted I–V characteristics, at least one subcell is not illuminated externally. In the absence of optical coupling, the series-connected triple-junction cell would not deliver any current in these cases.

At short circuit $V_{ext} = 0$ V of the red curve (circle symbols) in Figure 2, where only the top and middle cells are externally illuminated, the top and middle cells are close to their individual open circuit voltages $V_{oc,top}$ and $V_{oc,mid}$, and the bottom cell is in reverse $V_{bot} = -(V_{oc,top} + V_{oc,mid})$. As the top and middle cells are in forward bias, there is radiative recombination in both subcells. The photons

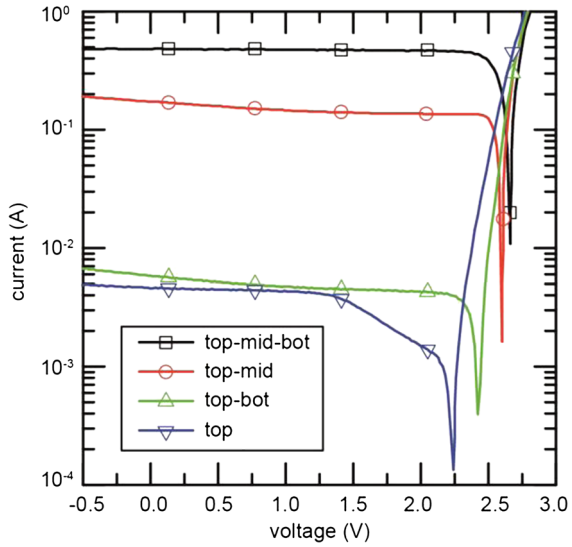

Figure 2. I–V curves of a 30.2 cm^2 $Ga_{0.50}In_{0.50}P/Ga_{0.99}In_{0.01}As$/Ge triple-junction solar cell with illuminated top, middle, and bottom cells in black (squared symbols), illuminated top and middle cells in red (circle symbols), illuminated top and bottom cells in green (triangle top symbols), and only top cell illumination in blue (triangle down symbols).

emitted by the top cell are absorbed in the middle cell. The increase of $V_{oc,mid}$ by this effect, however, is negligible for all practical purposes. More importantly, a fraction of the photons emitted by the middle cell are absorbed in the bottom cell and result in a photocurrent there. This optical coupling photocurrent, quantified by Eq. (5), together with the reverse current in the bottom junction is responsible for the relatively high short circuit current of the whole solar cell. The same explanation holds for the green I–V curve (triangle up symbols) in Figure 2, where only the top and bottom cells are externally excited. In this case, the optical coupling from the top to the middle cell has the main influence on the short circuit current.

A different situation appears for the blue I–V (triangle down symbols) characteristic in Figure 2, where only the top cell is illuminated. For a large voltage range, the top cell stays near its $V_{oc,top}$ and is responsible for optical coupling into the middle cell. This leads to a situation similar to the green curve (triangle up symbols). In this case, however, the bottom cell is not illuminated externally, and only the optical coupling current $I_{oc,bot}$ from the middle to the bottom cell is available. In this situation, the bottom cell is in reverse for almost the entire voltage range of the I–V curve. There is a relatively strong increase for the external current between $V_{oc,ext}$ and 1.4 V because of the non-ideal reverse characteristic of the limiting bottom cell. The same is true for the red curve (circle symbols), where the bottom cell was also biased in reverse. The apparent difference in slope is only owed to the logarithmic representation of the current in Figure 2. At about 1.4 V for the blue curve (triangle down symbols), the reverse current in the bottom cell is equal to the optical coupling current generated in the middle cell, and a middle cell limitation takes over for lower external voltages. The slight current increase towards small voltages reflects the reverse characteristic of the middle cell. This reverse characteristic is even more pronounced in the green I–V curve (triangle up symbols), where higher reverse voltages are applied to the middle cell, because of the additional external bottom cell illumination.

Finally, the strong influence of the optical coupling on the I–V curves is also visible in the large open circuit voltages that can be readout at the sharp kink in the logarithmic graphs. The open circuit voltage of almost 2.25 V for an only top cell illuminated triple-junction is significantly higher than the one of a $Ga_{0.50}In_{0.50}P$ top cell, which is approximately 1.4 V. The cell presented here is a good example for a non-ideal cell where the extraction of the photocurrents at short circuit leads to significant inaccuracies.

3. DISCUSSION

Except for the voltage range where a reverse characteristic is dominating the I–V curve, all curves of Figure 2 can be described by the equivalent circuit of Figure 1. This requires six different dark saturation currents, two for each subcell, and the two coupling efficiencies η_{tm} and η_{mb}. A simple computational fit of a single curve cannot lead to a reliable result because of the high number of unknown fitting parameters.

Optical coupling, however, can be used to extract information on the individual subcells of the multijunction solar cell. This reduces the number of free parameters drastically and results in subcell I–V parameters with high reliability. The enabling factor is the fact that the optical coupling current is constant over a certain voltage range because of the essentially fixed biasing conditions of the exciting subcell. Without restricting the general validity, the following equations are derived for the case of optical coupling between top and middle cells. They can be applied to the optical coupling between middle and bottom cells equivalently.

For $\exp(qV/kT) \gg 1$, Eqns (1) and (5) can be combined to

$$I_{top}(V_{top}) = I_{ph,top} - \frac{I_{01,top}}{C_{tm}} I_{oc,mid}(V_{top}) - \frac{I_{02,top}}{C_{tm}^{1/2}} I_{oc,mid}^{1/2}(V_{top}) \quad (10)$$

for any given biasing point V_{top} of the top cell. If only the top and bottom cells are externally illuminated with $I_{ph,top}$ and $I_{ph,bot}$ as well as the condition $I_{ph,bot} \gg I_{oc,mid}$ holds, the triple-junction I–V curve is governed by the I–V curve of the middle cell.

In order to evaluate Eq. (10) further, an appropriate biasing point on the I–V curve of the complete triple-junction cell has to be chosen. A suitable choice is $V_{ext} = V_{oc,TJ} - V_{oc,mid}$, where $V_{oc,TJ}$ represents the open

circuit voltage of the entire cell under the given illumination conditions and $V_{oc,mid}$ the corresponding quantity of the middle cell. Because $I_{oc,mid} < I_{ph,top}$, as shown before, the middle cell is close to short circuit conditions at this operating point. Thus, $I_{oc,mid}$ equals $I_{sc,mid}$. Furthermore, because the middle cell is limiting the overall current, I_{top} and $I_{sc,mid}$ equal $I_{ext} = I_{TJ}(V_{ext})$. Thus, Eq. (10) can be expressed as merely a function of the external current of the triple-junction cell I_{ext} at this particular biasing point:

$$I_{ext} = I_{ph,top} - \frac{I_{01,top}}{C_{tm}} I_{ext} - \frac{I_{02,top}}{C_{tm}^{1/2}} I_{ext}^{1/2} \tag{11}$$

Eq. (11) can be further simplified to

$$\begin{aligned} I_{ph,top} &= \alpha_{tm} I_{ext} + \beta_{tm} I_{ext}^{1/2} \text{ with } \alpha_{tm} \\ &= \frac{I_{01,top}}{C_{tm}} + 1 \text{ and } \beta_{tm} = \frac{I_{02,top}}{C_{tm}^{1/2}} \end{aligned} \tag{12}$$

α_{tm} and β_{tm} can be determined by fitting of Eq. (12) when I_{ext} is measured for different $I_{ph,top}$. This leads to a fixed relation between $I_{01,top}$ and $I_{02,top}$, as derived by Reference [20] in a different approach:

$$I_{02,top} = \beta_{tm} \left(\frac{I_{01,top}}{\alpha_{tm} - 1} \right)^{1/2} \tag{13}$$

and the coupling efficiency η_{tm}, based on its definition in Eq. (6), can be expressed as

$$\eta_{tm} = \frac{1}{\alpha_{tm} - 1} \tag{14}$$

With the help of Eqns 12–14, a relation between the two diode parameters of a subcell and the optical coupling efficiency η can be obtained. By changing the illumination intensity for the exciting subcell, $I_{ph,top}$, the corresponding biasing voltage and consequently the optical coupling current can be varied.

As mentioned before, $I_{ext} = I_{TJ}(V_{ext})$ has to be evaluated at the biasing point $V_{ext} = V_{oc,TJ} - V_{oc,mid}$. This biasing point, which can also be written as the sum of top and bottom cell open circuit voltages, however, is not known exactly. It can only be estimated, with an uncertainty V_d. Quantitatively, the slope of the complete I–V curve around V_{ext} is governed by the shunt resistance $R_{shunt,mid}$ of the middle cell. This shunt resistance introduces an uncertainty of $V_d/R_{shunt,mid}$ in the determination of the appropriate I_{top} by I_{ext} in the left side of Eq. (10) and similarly the same uncertainty in the determination of $I_{oc,mid}$ by I_{ext}. Therefore, in order to measure $I_{oc,mid}$ accurately by I_{ext} in the presence of an uncertainty in the biasing point, the condition

$$\frac{V_d}{R_{shunt,mid}} \ll I_{oc,mid} \tag{15}$$

has to hold.

If this is the case, then the uncertainty in V_{ext} does not translate into an uncertainty in V_{top} big enough to affect $I_{oc,mid}$ on the right side of Eq. (10) in addition: because $I_{oc,mid}$ is lower than $I_{ph,top}$, the operating point V_{top} is close to $V_{oc,top}$, and in particular the slope of the top cell I–V curve at V_{top} can be approximated by the slope at $V_{oc,top}$:

$$\left. \frac{\partial V}{\partial I} \right|_{V_{top}} = -\frac{kT}{q} \frac{1}{I_{ph,top}} \tag{16}$$

if in this case the ideal one-diode model is applied for simplicity. The uncertainty in the external biasing point V_d thus translates into an uncertainty of ΔV_{top} for the biasing point of the top cell of

$$\Delta V_{top} = \frac{kT}{q} \frac{V_d}{I_{ph,top} R_{shunt,mid}} \tag{17}$$

and consequently into an uncertainty $\Delta I_{oc,mid}$ of the optical coupling current

$$\Delta I_{oc,mid} = I_{oc,mid} \frac{V_d}{I_{ph,top} R_{shunt,mid}} \tag{18}$$

according to Eq. (7) in a linear approximation.

Making use of the fact that $I_{oc,mid}$ is smaller than $I_{ph,top}$ results in

$$\Delta I_{oc,mid} < \frac{V_d}{R_{shunt,mid}} \tag{19}$$

Therefore, if Eq. (15) is fulfilled, the impact of the voltage uncertainty in V_{top} is negligible and does not translate in an additional, unacceptable uncertainty in $I_{oc,mid}$.

In Figure 3, the measurement principle just outlined is illustrated graphically. For the top cell in Figure 3a, I_{ext} is measured for a set of I–V curves at an external voltage of approximately $V_{oc,TJ} - V_{oc,mid}$ with constantly high illumination of the bottom cell and varying intensity for the top cell. $I_{ph,top}$ is determined in separate measurements at $V_{oc,TJ} - \mathrm{V_{oc,top}}$ with an additional external illumination of the middle cell to ensure top cell limitation. A very similar approach is applied for the middle cell in Figure 3b. I_{ext} is measured at $V_{oc,TJ} - V_{oc,bot}$ for different illumination levels of the middle cell, while the top cell is constant and highly illuminated, and for the determination of $I^*_{ph,mid}$ at $V_{oc,TJ} - V_{oc,mid}$, the bottom cell is externally excited as well. For the middle cell, these conditions result in an additional, secondary optical coupling contribution from top to middle cell, which will be dealt with later on.

In Figure 4a, several I–V curves with constant bottom cell illumination, no external middle cell illumination, and different top cell illuminations are shown. These triple-junction I–V characteristics are dominated by the optical coupling current and the reverse current in the middle cell for voltages lower than the open circuit voltage. As argued previously, I_{ext} has to be evaluated at $V_{ext} = V_{oc,TJ} - V_{oc,mid}$. $V_{oc,TJ}$ can be simply read from the kink in

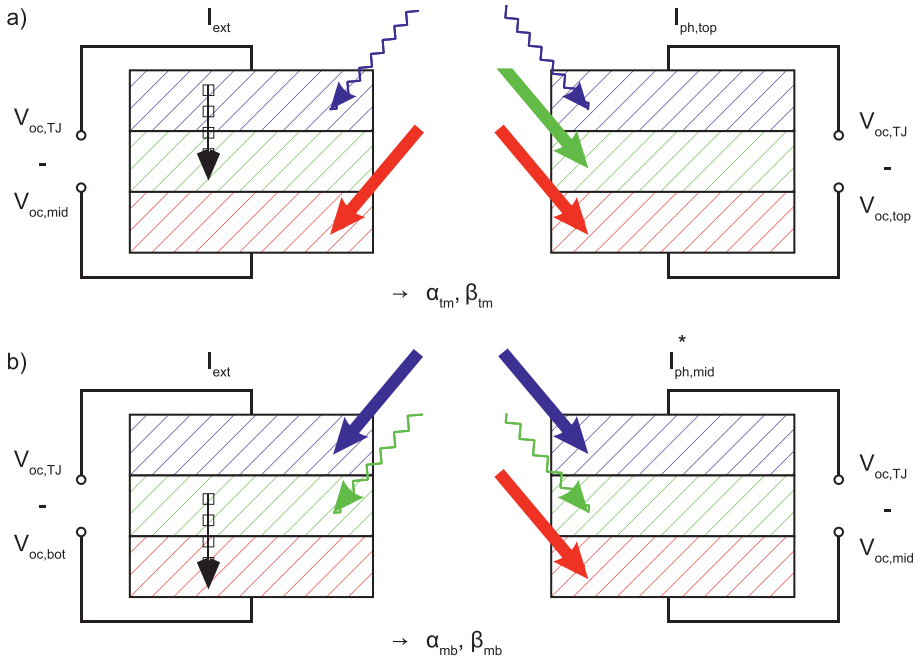

Figure 3. Illustration of the measurement principle for (a) the top cell and (b) the middle cell. The drawings on the left visualize the measurement conditions for I_{ext} and the ones on the right for I_{ph}. The relevant biasing conditions are also included. Bold arrows denote constant, high illumination intensities, whereas the curved arrows indicate a variation in the intensity. Optical coupling is represented by black arrows with squares.

the logarithmic I–V curve. The exact value of $V_{oc,mid}$ is not known. A good approximation for the open circuit voltage of any subcell is $E_g/q - 0.4\,\mathrm{V}$, where E_g represents the bandgap energy [31]. According to Figure 4a, the optical coupling currents, evaluated as I_{ext}, are approximately a factor 100 lower than typical 1 sun photocurrents, resulting in another reduction of the open circuit voltage by 0.1 V.[2] In summary, $V_{oc,mid}$ can be estimated at 0.9 V, with an uncertainty V_d of approximately 0.1 V. By evaluating the external current at this biasing point, I_{ext} can be extracted at the positions marked by black dots in Figure 4a. In a non-logarithmic representation, the inverse slope at this biasing point and thus $R_{shunt,mid}$ can be determined as 3.3 kΩ. This value for the shunt resistance is very similar for each I–V curve. The uncertainty in I_{ext} is thus estimated as 30 µA according to Eq. (15), which translates into 9% uncertainty for the lowest I_{ext} shown in Figure 4.

In order to apply Eq. (12), the photocurrents of the top cell, $I_{ph,top}$, for the different illumination settings have to be known as well. Those were determined in a separate measurement. The I–V curve of the cell was measured for the required top cell illumination conditions, but with an external middle cell illumination adjusted such that the top cell is current limiting. The exact $I_{ph,top}$ can be read out at an external voltage of $V_{ext} = V_{oc,TJ} - V_{oc,top}$, where there is no voltage drop over the top cell. $V_{oc,top}$ can be estimated from the 1.88 eV bandgap of the $Ga_{0.50}In_{0.50}P$ top cell to about 1.4 V [31]. The shunt resistance for the top cell $R_{shunt,top}$ derived from the measured slope of all the I–V curves at this value of V_{ext} is in contrast to $R_{shunt,mid}$ not constant. It decreases from around 1 kΩ at photocurrents $I_{ph,top}$ below 100 mA to values around 100 Ω at 500 mA photocurrent. Such a photocurrent-dependent change in slope can in principle be modeled by a certain region of the top cell that is dominated by the $n = 2$ diode and connected by an appropriate series resistance to the remainder of the cell. This, however, is beyond the scope of this paper. Again with $V_d = 0.1$ V, Eq. (15), and the corresponding shunt resistances $R_{shunt,top}$, the uncertainty in $I_{ph,top}$ is about 0.2% for all conditions, which is below the uncertainty of the measurement device of 1%.

The pairs of $I_{ph,top}$ and I_{ext} obtained in this way are plotted in Figure 4b. They can be fitted to Eq. (12) very well and result in α_{tm} of 81.7 and β_{tm} of 1.8 $\mathrm{A}^{1/2}$.

Equations 12–14 can be applied equivalently for the coupling of middle cell to the bottom cell. In Figure 5a, the respective I–V curves with constant top cell illumination, varying middle cell illumination, and no external bottom cell illumination are shown.

The appropriate biasing point $V_{ext} = V_{oc,TJ} - V_{oc,bot}$ to determine I_{ext} can be estimated from the bandgap of 0.66 eV and supported by experience with single-junction Ge cells to be about 0.2 V smaller than the triple-junction open circuit voltage. While this is in general a good approximation, for the cell investigated here, the shunt

[2] With $V_{oc} = kT/q * ln(I_{ph}/I_0)$ and $kT/q = 25$ mV, a $\Delta V_{oc} = 25$ mV * ln (100) results and evaluates to 115 mV.

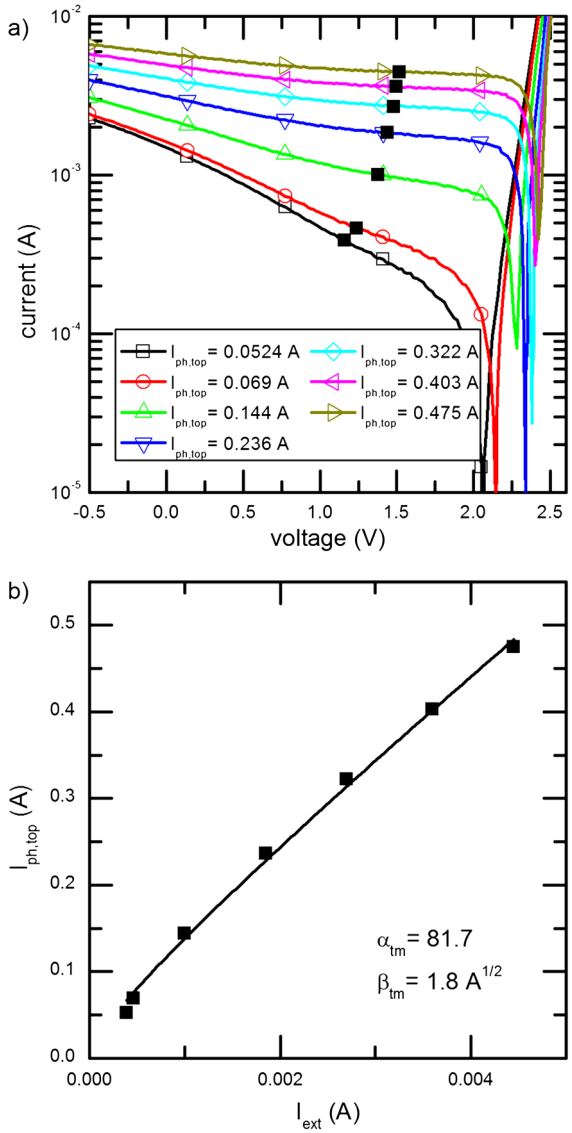

Figure 4. (a) Top and bottom cell illuminated triple-junction I–V curves with different $I_{ph,top}$ and a constant $I_{ph,bot}$ of 1.342 A. (b) The corresponding fit of the $I_{ph,top}$ and I_{ext} pairs to Eq. (12), evaluated at $V_{oc,TJ} - 0.9$ V.

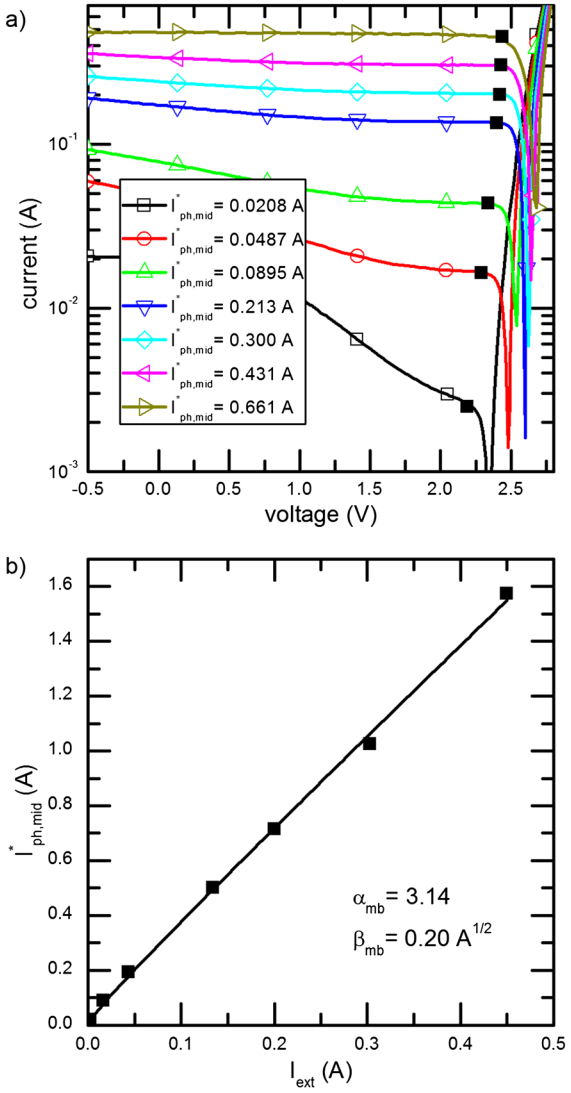

Figure 5. (a) Top and middle cell illuminated triple-junction I–V curves for different photocurrents of the middle cell including the optical coupling contribution from the top cell, $I^*_{ph,mid}$, and constant $I_{ph,top} = 0.475$ A. (b) The corresponding fit of the $I_{ph,mid}$ and I_{ext} pairs to Eq. (12), evaluated at $V_{oc,TJ} - 0.2$ V.

resistance present in the bottom cell affects the open circuit voltage for the lowest illumination levels. The estimated open circuit voltage for the bottom cell was reduced by 50 mV to 0.15 V in these cases. This was later verified with the help of the pulsed bottom cell V_{oc} measurements. Using again $V_d = 0.1$ V, Eq. (15), and $R_{shunt,bot} = 430\,\Omega$, which is similar for each I_{ext}, derived from the measured slope of the I–V curves at this position, the uncertainty in I_{ext} is determined to 0.23 mA, which results in an uncertainty of 9% for the lowest I_{ext}.

The determination of the middle cell photocurrent $I^*_{ph,mid}$ from separate I–V curve measurements, where the middle cell is current limiting, is more complex in comparison with $I_{ph,top}$. The middle cell photocurrent $I^*_{ph,mid}$ is always the sum of the externally generated current $I_{ph,mid}$ due to the laser illumination and the optical coupling current $I_{oc,mid}$ from the top to the middle cell. Because $I_{ph,top}$ was kept constant at its maximum value for all measurements, this effect plays a role for the lowest external middle cell illumination intensities. In this middle cell-limited scenario, the method outlined earlier for the determination of $I_{ph,top}$ can be applied equivalently. The optical coupling contribution is automatically included in this case. An appropriate biasing point is 0.9 V smaller than the open circuit voltage as outlined previously. It has to be noted that this procedure neglects the fact that the top cell is at slightly different biasing points for the I_{ext} and $I^*_{ph,mid}$ measurements because of the different amount of current that is

extracted from the cell in the two measurements. For the cell presented here, with a relatively low coupling efficiency between top and middle cells, this is negligible.

In case of cells with a high coupling efficiency between top and middle cells, however, a modified determination of I_{ext} and $I^*_{ph,mid}$ has to be used. It is schematically illustrated in Figure 6 for the determination of I_{ext}. A given external illumination of the middle cell results in a certain optical coupling current in the bottom cell. Starting with zero illumination of the top cell and continuously increasing the top cell illumination, the top cell current is limiting the overall current, and there is no optical coupling contribution from top to middle cell. The appropriate biasing condition is $V_{oc,TJ} - V_{oc,top}$ in this case. Likewise, starting from high top cell illumination levels and decreasing the top cell illumination gradually, the bottom cell is limiting the current. Therefore, $V_{oc,TJ} - V_{oc,bot}$ is an appropriate biasing point. In this situation, there is an additional optical coupling contribution from top to middle cell. At the intersection of both $I_{ext} - I_{ph,top}$ curves, coming from low and high $I_{ph,top}$ values, the photocurrent in the top cell exactly matches the optical coupling current in the bottom cell, and there is no unwanted optical coupling contribution from top to middle cell anymore. This point of exact current match between top and middle cells, visualized by the red dot in Figure 6, is hard to be achieved experimentally. In the regions to the left and the right of this point, however, the experimental determination is unambiguous, and the crossover point can be clearly identified.

For the determination of $I_{ph,mid}$, the procedure is identical. In this case, the bottom cell is at a constant, high illumination level. Starting from low top cell illumination levels, the cell current is measured at $V_{oc,TJ} - V_{oc,top}$. As before, in this case, the top cell is limiting the overall current, and there is no optical coupling contribution into the middle cell. From the opposite direction, the cell current is measured as a function of decreasing top cell illumination at $V_{oc,TJ} - V_{oc,mid}$. At the cross-over point, there is again current match between top and middle cells, and $I_{ph,mid}$ can be inferred without any optical coupling contribution from the top cell.

An additional technical difficulty arose from the setup used in this work. The illumination intensity achievable for the top cell was limited by the LED array, to an equivalent $I_{ph,top} = 0.475$ A for the cell investigated, while middle cell photocurrents of up to 1.5 A could be reached with the laser illuminating the middle cell. In the $I^*_{ph,mid}$ determination used for this cell, with $I_{ph,top}$ remaining constantly at its maximum value, a point will be reached where the measured triple-junction current does not change any more with further increase of the middle cell illumination. At this point, the known $I_{ph,top}$ equals $I^*_{ph,mid}$. For higher middle cell laser intensities, the middle cell photocurrent was linearly scaled from this starting point. For illumination intensities in this range, characterized by an $I_{ph,mid}$ comparable with $I_{ph,top}$ or higher, the optical coupling contribution into the middle cell is negligible. The uncertainty of 30 μA for the measurement of middle cell-limited external currents determined previously is negligible for the measurement of the laser-generated photocurrents in comparison with the uncertainty of the source–measure unit of 1%.

The $I^*_{ph,mid}$ and I_{ext} data points are plotted in Figure 5b. They can again be fitted to Eq. (12) very well and result in α_{mb} of 3.14 and β_{mb} of 0.20 $A^{1/2}$. Because of the nearly

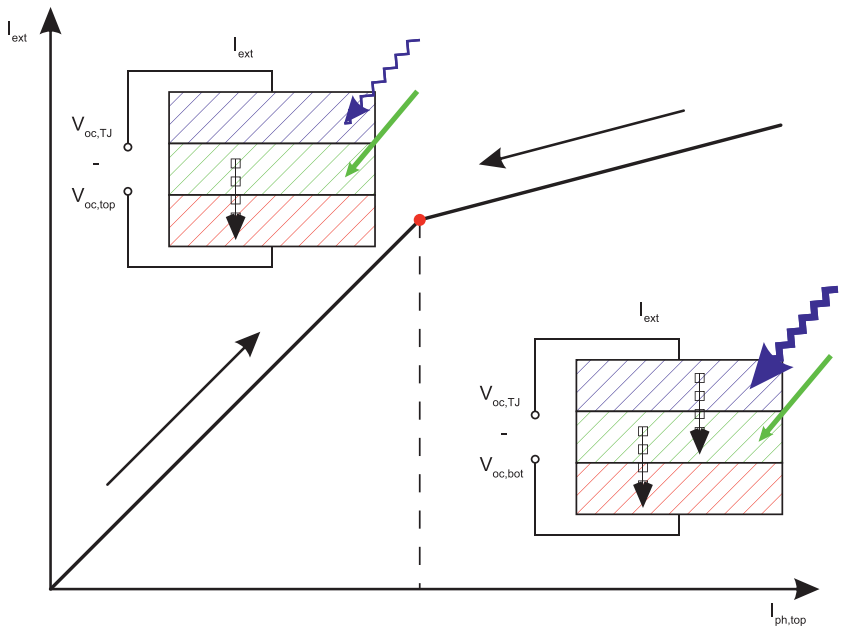

Figure 6. Schematic description of the determination of I_{ext} for cells with high coupling efficiency between top and middle cells.

linear behavior, the parameter β_{mb}, which addresses the contribution of diode 2, has a comparatively higher uncertainty.

For the bottom cell, whose voltage information cannot be measured by an optical coupling current, a similar procedure based on PL is used. By combining Eq. (1) and the integrated PL intensity Φ_{bot} from Eq. (2), an equivalent expression to Eq. (12) can be found for open circuit conditions:

$$I_{ph,bot} = \alpha_b \Phi_{bot} + \beta_b \Phi_{bot}^{1/2} \text{ with } \alpha_b = \frac{I_{01,bot}}{C_b} \text{ and } \beta_b = \frac{I_{02,bot}}{C_b^{1/2}} \quad (20)$$

with the constant C_b defined as

$$C_b = \int EQE_{bot}(E)\varphi_{BB}(E)dE \quad (21)$$

There is again a fixed relation between $I_{01,bot}$ and $I_{02,bot}$ given by

$$I_{02,bot} = \beta_b \left(\frac{I_{01,bot}}{\alpha_b}\right)^{1/2} \quad (22)$$

In Figure 7, this measurement principle is illustrated graphically. For different intensities of the 975-nm laser PL intensity Φ_{bot} images are acquired. In addition, the corresponding photocurrents $I_{ph,bot}$ in the bottom cell are required. Choosing an external biasing condition of $V_{oc,TJ} - V_{oc,bot}$, $I_{ph,bot}$ is determined similarly to the middle cell photocurrent by applying equal photocurrents in top and middle cells and gradually increasing the bottom cell illumination. Looking at the external short circuit current, a laser intensity can be found where $I_{ph,bot}$ is identical to the top and middle cell ones. In this situation, all subcells are biased at short circuit, and there is no optical coupling contribution to $I_{ph,bot}$. This is important because for the PL images, the middle cell is not excited, and no additional optical coupling current from the middle cell has to be taken into account. The required bottom cell photocurrents are then linearly scaled with the laser intensity based on this data point.

Such a measurement concept based on the PL emission of the individual subcells is also valid for top and middle cells but has the disadvantage that the optical coupling efficiencies η are not extracted automatically in contrast to Eq. (12). The bottom cell PL intensity Φ_{bot} is detected at open circuit conditions with a HgCdTe CCD camera [7]. As shown in Figure 8a, the bottom cell luminescence images are usually homogeneous, and it is a good assumption to average the intensity over the whole cell area. The black dots are defect pixels of the CCD sensor. For the bottom PL images, the top and middle cells are not excited.

To be able to fit the measured PL intensities to Eq. (20), the corresponding photocurrents $I_{ph,bot}$, which are generated by the 975-nm laser, were determined as outlined previously. The $I_{ph,bot}$ and Φ_{bot} data points obtained, together with the corresponding fit of Eq. (20), are plotted in Figure 8b. The PL intensity measurement with the CCD camera is in arbitrary units (a.u.), which implies that only the relation between α_b and β_b can be determined, but not their absolute values. The very linear behavior indicates that the bottom cell pn-junction can essentially be described by a one-diode model.

With the help of this measurement series and the fitting of the individual subcells according to Figures 4, 5, and 8, a relationship between the two diode parameters in each subcell is derived. In addition, with the help of Eq. (14), also both optical coupling parameters are obtained. In Table I, these results are summarized. The number of unknown parameters in the equivalent circuit of Figure 1 has been reduced from 8 to 3.

To determine the remaining parameters, a current/voltage pair is required for each subcell. Ideally, the open circuit voltage is chosen, where disturbing effects like the series resistance do not play a role. Starting with the bottom subcell, theoretically it is possible to measure the open circuit voltage when only the bottom cell is illuminated. Together with the previously measured photocurrent for the corresponding illumination, $I_{01,bot}$ could be determined based on Eq. (1). In practice, however, every voltmeter has a finite internal resistance and thus requires a certain current flow for the voltage measurement to take place. As the top and middle subcells are not illuminated, this current is not able to flow continuously, and such a steady-state measurement is not possible.

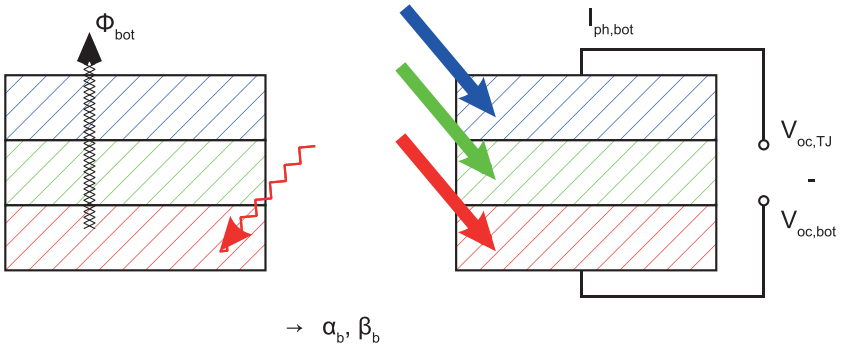

Figure 7. Schematic illustration of the measurement principle for the bottom cell.

DOI: 10.1002/pip

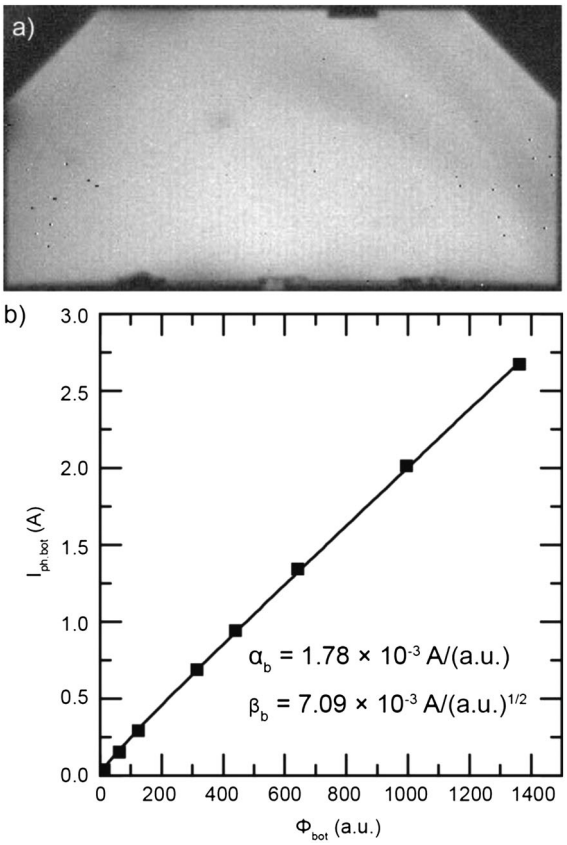

Figure 8. (a) Photoluminescence image of the bottom cell at $I_{ph,bot} = 0.942$ A. (b) The corresponding fit of the $I_{ph,bot}$ and Φ_{bot} pairs to Eq. (20).

The capacitance of the middle and top pn-junctions, however, can be exploited for a pulsed measurement of the desired open circuit voltage. This has been outlined in detail in Reference [24]. Figure 9a shows the corresponding equivalent circuit for the time-resolved measurement. Figure 9b illustrates the time-resolved open circuit voltage during a single 0.5 ms pulse of the 975-nm laser with the shortest rise time achievable experimentally, and in Figure 9c, the same measurement is depicted for the 803-nm middle cell laser. The time resolution was 2 µs in both cases, and only the first pulse was measured to avoid additive charging effects by subsequent pulses.

The typical capacitance of the single subcells is in the range of 2 µF, as argued in Reference [24] and taking into account the larger cell size, while the laser intensity for the depicted 975-nm pulse corresponds to a photocurrent of 0.942 A. Therefore, the bottom cell open circuit voltage is already built up after several µs. Next to this very fast rise time, which is in the same order of magnitude as the rise time of the laser intensity itself, an additional small linear increase of the open circuit voltage is observed in Figure 9b. This can be explained by parasitic absorption in top or middle cell. With the help of a $Ga_{0.99}In_{0.01}As$ single-junction cell, it was verified that the 975-nm photons are absorbed at impurities there [32] and result in a photocurrent in the range of 10 µA in the middle cell. Because this photocurrent is orders of magnitude smaller than the photocurrent of the bottom cell under external illumination, the buildup of an open circuit voltage in the middle cell takes place on a much longer timescale.

At the end of the 0.5 ms laser pulse, a contribution of about 5 mV from the middle cell results, but at the beginning of the plateau, it is well below 1 mV and thus can be neglected. It is important to note that in case of even weakly shunted middle cells, this effect results in no measurable open circuit contribution any more. Likewise, for lower intensities of the 975-nm laser, this effect is even less pronounced. The open circuit voltage of the bottom cell in Figure 9b is derived at this point in time to 0.242 V. The photocurrent generated in bottom and middle cell results in a charging and the buildup of a voltage of opposite polarity in the top cell. The measurement device has an internal resistance of 1 MΩ. Combined with the top cell capacity around 2 µF, this leads to an RC time constant of 1 s. Therefore, even at the end of the pulse, a negligible voltage drop below 1 mV at the top cell is found. Using the photocurrent/open circuit voltage pair determined (0.942 A, 0.242 V) and Eq. (1) together with the $I_{01,bot}/I_{02,bot}$ ratio according to Table I, $I_{01,bot} = 6.7 \times 10^{-5}$ A is found.

An equivalent time-resolved measurement is performed with the 803-nm laser for the middle cell. Because of optical coupling, the combined open circuit voltage $V_{oc,mb}$ of the middle and bottom subcells is measured. In the measurement shown in Figure 9c, the laser intensity corresponds to a photocurrent of 0.500 A in the middle cell. Because of the high internal resistance of the voltmeter, the cell is virtually in open circuit condition again. An upper limit of the corresponding optical coupling current can be approximated by 0.5 * 0.500 A, based on the coupling efficiency determined and the assumption that most of the current is flowing through the first diode characterized by $I_{01,mid}$ in that voltage regime. Therefore, again only µs are required for the buildup of the open circuit voltage of the middle and bottom subcells. Also in this situation, the charging of the top cell capacitance enables a short-term current flow and consequently voltage measurement. The resulting time-dependent voltage measurement is shown in Figure 9c. Again, because of the much longer charging time constant of the top cell, the measured open circuit voltage is affected by less than 1 mV at the end of the 0.5 ms laser pulse.

Table I. Fitting parameters α and β as well as the resulting optical coupling parameters η and the relationship between I_{02} and I_{01}.

Top	$\alpha_{tm} = 81.7$	$\beta_{tm} = 1.8\ \mathrm{A}^{1/2}$	$\eta_{tm} = 0.012$	$I_{02,top} = 0.20\ \mathrm{A}^{1/2} \cdot I_{01,top}^{1/2}$
Middle	$\alpha_{mb} = 3.14$	$\beta_{mb} = 0.20\ \mathrm{A}^{1/2}$	$\eta_{mb} = 0.467$	$I_{02,mid} = 0.14\ \mathrm{A}^{1/2} \cdot I_{01,mid}^{1/2}$
Bottom	$\alpha_b = 1.78 \times 10^{-3}$ A/(a.u.)	$\beta_b = 7.09 \times 10^{-3}$ A/(a.u.)$^{1/2}$	—	$I_{02,bot} = 0.17\ \mathrm{A}^{1/2} \cdot I_{01,bot}^{1/2}$

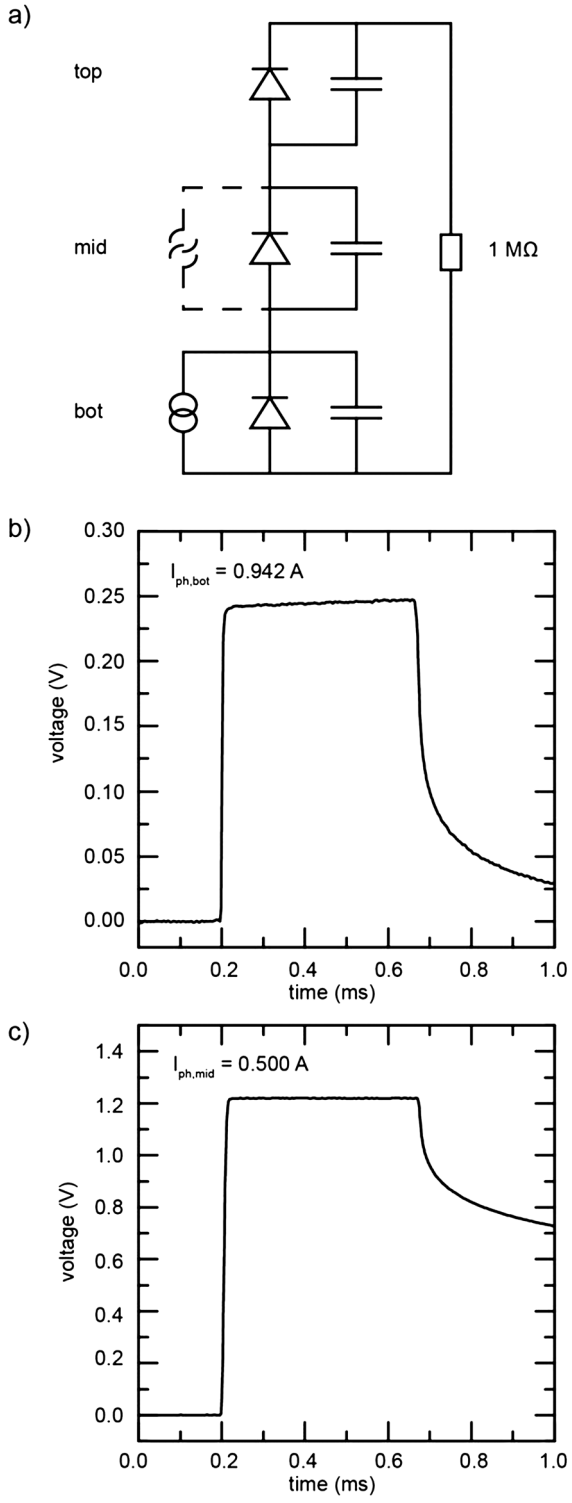

Figure 9. (a) Equivalent circuit for the voltage measurement during a pulsed laser illumination of the bottom subcell and with additional parasitic absorption in the middle cell. (b) Time-resolved open circuit voltage measurements for a 975-nm laser pulse with $I_{ph,bot} = 0.942$ A and (c) an 803-nm laser pulse with $I_{ph,mid} = 0.500$ A.

With the help of the derived open circuit voltage of middle and bottom cell $V_{oc,mb} = 1.218$ V, the following set of four equations can be solved:

$$\begin{aligned} &I_{01,bot}e^{\frac{qV_{oc,bot}}{kT}} + I_{02,bot}e^{\frac{qV_{oc,bot}}{2kT}} = \eta_{mb}I_{01,mid}e^{\frac{qV_{oc,mid}}{kT}} \\ &I_{01,mid}e^{\frac{qV_{oc,mid}}{kT}} + I_{02,mid}e^{\frac{qV_{oc,mid}}{2kT}} = I_{ph,mid} \\ &V_{oc,bot} + V_{oc,mid} = V_{oc,mb} \\ &I_{02,mid} = 0.14I_{01,mid}^{1/2} \end{aligned} \tag{23}$$

Next to $V_{oc,mb}$, the bottom cell parameters $I_{01,bot}$, $I_{02,bot}$, the coupling coefficient η_{mb}, and the laser-generated $I_{ph,mid}$ are already well known in Eq. (23). Numerically solving Eq. (23) yields the unknown parameters $V_{oc,bot}$, $V_{oc,mid}$, and $I_{01,mid}$ and $I_{02,mid}$. $I_{01,mid}$ is obtained as 2.8×10^{-18} A.

The only remaining unknown parameter of the equivalent circuit in Figure 1 is $I_{01,top}$ of the top cell. This can be calculated from the open circuit voltage $V_{oc,TJ} = 2.662$ V of the entire cell under steady-state illumination conditions with $I_{ph,bot} = 0.475$ A, $I_{ph,mid} = 0.500$ A, and $I_{ph,top} = 1.342$ A. The following set of equations is obtained.

$$\begin{aligned} &I_{01,bot}e^{\frac{qV_{oc,bot}}{kT}} + I_{02,bot}e^{\frac{qV_{oc,bot}}{2kT}} = \eta_{mb}I_{01,mid}e^{\frac{qV_{oc,mid}}{kT}} + I_{ph,bot} \\ &I_{01,mid}e^{\frac{qV_{oc,mid}}{kT}} + I_{02,mid}e^{\frac{qV_{oc,mid}}{2kT}} = \eta_{tm}I_{01,top}e^{\frac{qV_{oc,top}}{kT}} + I_{ph,mid} \\ &I_{01,top}e^{\frac{qV_{oc,top}}{kT}} + I_{02,top}e^{\frac{qV_{oc,top}}{2kT}} = I_{ph,top} \\ &V_{oc,bot} + V_{oc,mid} + V_{oc,top} = V_{oc,TJ} \\ &I_{02,top} = 0.20I_{01,top}^{1/2} \end{aligned} \tag{24}$$

By solving Eq. (24) for the five unknown parameters $V_{oc,bot}$, $V_{oc,mid}$, $V_{oc,top}$, $I_{01,top}$, and $I_{02,top}$, $I_{01,top} = 2.3 \times 10^{-24}$ A is found.

This measurement principle is summarized schematically in Figure 10. Table II summarizes all parameters that define the equivalent circuit from Figure 1 for the measured triple-junction solar cell.

In order to verify the I–V parameters determined according to Table II, the equivalent circuit from Figure 1 is modeled with a simulation program with integrated circuit emphasis (SPICE) [33]. For the diode elements, the classical Berkeley SPICE diode model is used, and the optical coupling currents are modeled by current sources obeying the condition described by Eq. (7). The simulated I–V curves for the different illumination conditions in Figure 2 are shown in Figure 11a. Except for the influence of the reverse characteristics, which could not be taken into account, a good agreement between measurement and simulation is found. The optical coupling currents as well as the corresponding open circuit voltages are reproduced by the simulations.

As independent verification, the dark I–V characteristic of the simulated cell was measured and compared with

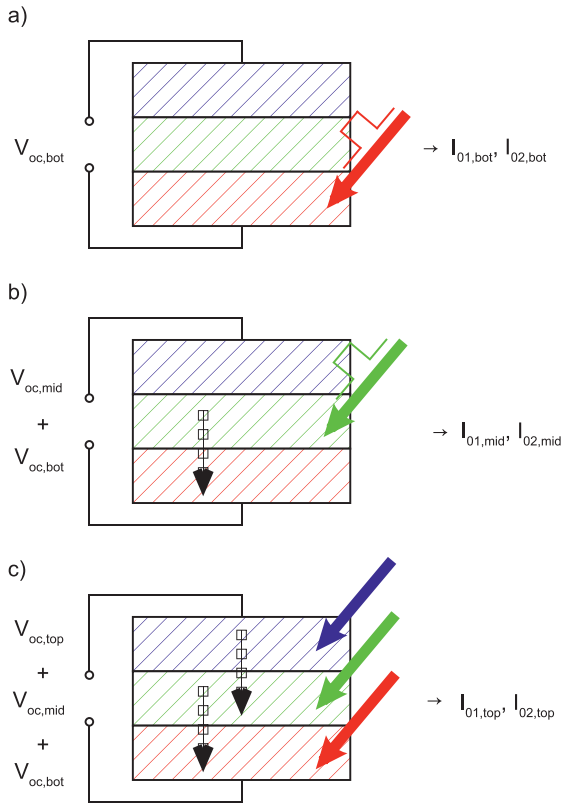

Figure 10. Illustration of the measurement principle to determine the open circuit voltages of the subcells, which are required to obtain absolute values of the dark saturation currents. (a) Pulsed illumination of the bottom cell. (b) Pulsed illumination of the middle cell resulting in additional optical coupling to the bottom cell. (c) The illumination of all three subcells can be performed at steady state. Optical coupling from top to middle and middle to bottom cell has to be taken into account.

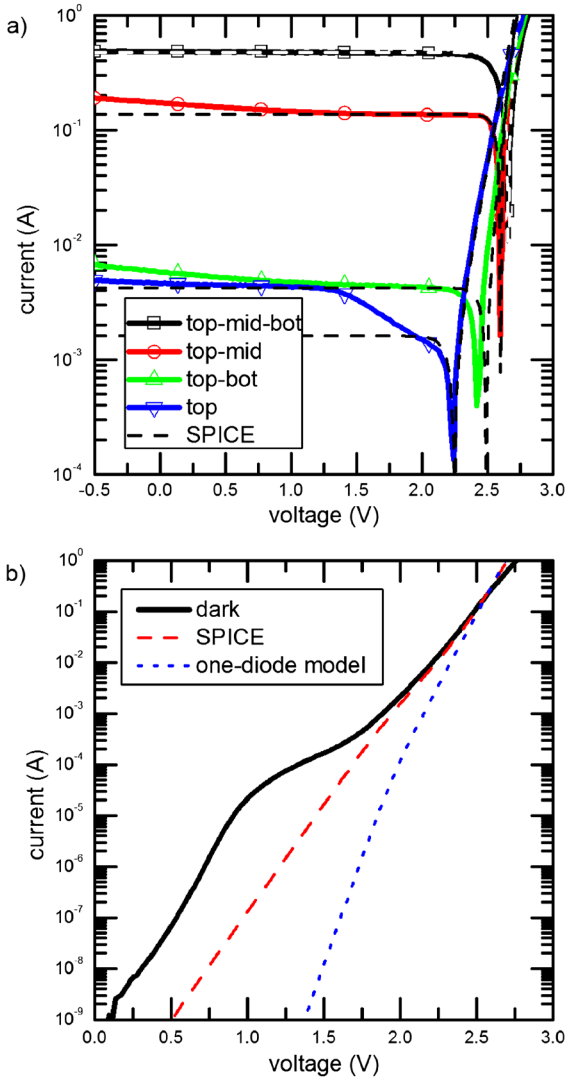

Figure 11. (a) I–V curves from Figure 2 together with corresponding simulation program with integrated circuit emphasis (SPICE) simulations with the diode parameters from Table II. (b) Measured and SPICE simulated dark I–V curve.

the simulated one in Figure 11b. A remarkable agreement in the current range between 1 and 300 mA is obtained, which confirms the validity of the method. The deviation for low currents is caused by shunts, which could not be taken into account in the simulation. The series resistance that is also not included in the simulations is responsible for the differences at high currents. Finally, the resulting dark I–V characteristic for a complete analysis based on an ideal one-diode model for each subcell is included in Figure 11b as well. Despite the relatively large uncertainties for I_{02}, especially for the bottom and middle subcells, it is essential to use the two-diode model to obtain good agreement with the measurement in the low current range as well.

In the top cell-limited cell design, the overall performance impact of optical coupling is limited. There is only a small increase in the fill factor because of the optical coupling from the middle to the bottom cell [22]. If the

Table II. I–V parameters determined for the $Ga_{0.50}In_{0.50}P/Ga_{0.99}In_{0.01}As/Ge$ triple-junction solar cell.

	I_{01} (A)	I_{02} (A)	η (–)
Top	2.3×10^{-24}	3.0×10^{-13}	0.012
Middle	2.8×10^{-18}	2.3×10^{-10}	0.467
Bottom	6.7×10^{-5}	1.4×10^{-3}	—

top cell is not the limiting subcell, however, optical coupling can recycle recombination losses in non-current-matched multijunction solar cells [23]. With the help of the SPICE model, it can be predicted that the effect of optical coupling increases the maximum power by 5.5% for the cell presented here under an assumed bottom cell-limited illumination spectrum with $I_{ph,top} = 500\,\text{mA}$, $I_{ph,mid} = 500\,\text{mA}$, and $I_{ph,bot} = 400\,\text{mA}$. For a concentration factor of 1000, the optical coupling improves the power for the same spectrum even by 7.7%. This improvement mainly originates from the higher short circuit current (+7.9%) and only slightly from the increased open circuit voltage (+0.4%). This points to the fact that optical coupling in general should be taken into account for the development of future multijunction cells with more junctions, especially under concentrated sunlight, as already pointed out [34,35].

4. CONCLUSION

The possibility to determine the subcell I–V characteristics using optical coupling and PL imaging is a valuable method for the characterization of multijunction solar cells. Accurate subcell I–V parameters are an essential input for quantitative SPICE network simulations [7]. The quality of shunt and sheet resistance characterization via those network simulations can be improved. The access to the subcell I–V curves is very valuable in degradation analyses under various environmental conditions. These can be performed directly on multijunction devices, and the detailed information of the individual subcells can be gained from the presented method. Therefore, no single-junction component cell sets are required, which never completely resemble the triple-junction cell stack. The method can be applied to solar cells with more junctions straightforwardly. The only prerequisite is to have an external light source for each junction that is not absorbed in another junction.

The method presented here to determine the subcell I–V parameters as well as optical coupling constants is strongly dependent on the possibility to read out the correct subcell photocurrents and optical coupling currents. For cells with low reverse currents, these currents can be extracted with ease in a relatively wide external voltage range. The uncertainties arising from non-ideal reverse characteristics can be directly assessed and quantified with the help of the measured I–V curves, which is a convenient feature of this method. For strong shunts, however, not only the uncertainties become larger, but optical coupling can be suppressed completely. In such a scenario, an estimate of the subcell diode parameters could be performed by PL measurements similar to the bottom cell procedure. But a strong shunt also results in non-negligible charging effects during the pulsed open circuit voltage determination, producing additional uncertainties there.

REFERENCES

1. Green MA, Emery K, Hishikawa Y, Warta W, Dunlop ED. Solar cell efficiency tables (version 45). *Progress in Photovoltaics: Research and Applications* 2015; **23**: 1–9.
2. Yamaguchi M, Takamoto T, Araki K, Ekins-Daukes N. Multi-junction III-V solar cells: current status and future potential. *Solar Energy* 2005; **79**: 78–85.
3. Banerjee A, Su T, Beglau D, Pietka G, Liu FS, Almutawalli S, Yang J, Guha S. High-efficiency, multijunction nc-Si:H-based solar cells at high deposition rate. *IEEE Journal of Photovoltaics* 2012; **2**: 99–103. DOI:10.1109/JPHOTOV.2011.2180892.
4. Ameri T, Dennler G, Lungenschmied C, Brabec CJ. Organic tandem solar cells: a review. *Energy & Environmental Science* 2009; **2**: 347–363.
5. Meusel M, Baur C, Létay G, Bett AW, Warta W, Fernandez E. Spectral response measurements of monolithic GaInP/Ga(In)As/Ge triple-junction solar cells: measurement artifacts and their explanation. *Progress in Photovoltaics: Research and Applications* 2003; **11**: 499–514. DOI:10.1002/pip.514.
6. Hoheisel R, Rönsch S, Dimroth F, Bett AW, Nesswetter H, Zimmermann CG. Electroluminescence exposes individual performances in multi-junction cells. *Compound Semiconductor* 2011; **17**: 28–31.
7. Nesswetter H, Lugli P, Bett AW, Zimmermann CG. Electroluminescence and photoluminescence characterization of multijunction solar cells . *IEEE Journal of Photovoltaics* 2013; **3**: 353–358. DOI: 10.1109/JPHOTOV.2012.2213801
8. Kirchartz T, Rau U, Hermle M, Bett AW, Helbig A, Werner JH. Internal voltages in GaInP/GaInAs/Ge multijunction solar cells determined by electroluminescence measurements. *Applied Physics Letters* 2008; **92**: 123502. DOI:10.1063/1.2903101.
9. Hoheisel R, Schachtner M, Stämmler E, Bett AW. Determination of the subcell photovoltage in multijunction solar cells via voltage-dependent capacitance analysis. *Applied Physics Letters* 2011; **98**: 251106. DOI:10.1063/1.3601468.
10. Adelhelm R, Bücher K. Performance and parameter analysis of tandem solar cells using measurements at multiple spectral conditions. *Solar Energy Materials and Solar Cells* 1998; **50**: 185–195. DOI:10.1016/S0927-0248(97)00143-8.
11. Tsuno Y, Hishikawa Y, Kurokawa K. Separation of the I–V curve of each component cell of multijunction solar cells. *Proceedings of the 31st IEEE Photovoltaic Specialists Conference (PVSC)* 2005; 1476.
12. Holovsky J, Bonnet-Eymard M, Boccard M, Despeisse M, Ballif C. Variable light biasing method to measure

component I–V characteristics of multi-junction solar cells. *Solar Energy Materials and Solar Cells* 2012; **103**: 128–133. DOI:10.1016/j.solmat.2012.04.014.

13. Lim SH, O´Brien K, Steenbergen EH, Li JJ, Ding D, Zhang YH. Analysis of spectral photocurrent response from multi-junction solar cells under variable voltage bias. *Proceedings of the 37th IEEE Photovoltaic Specialists Conference (PVSC)* 2010; 712.
14. Roensch S, Hoheisel R, Dimroth F, Bett AW. Subcell I-V characteristic analysis of GaInP/GaInAs/Ge solar cells using electroluminescence measurements. *Applied Physics Letters* 2011; **98**: 251113. DOI:10.1063/1.3601472.
15. Yoon H, King RR, Kinsey GS, Kurtz S, Krut DD. Bandgap engineering in high-efficiency multijunction concentrator cells. *3rd World Conference on Photovoltaic Energy Conversion Osaka* 2003; 745.
16. Baur C, Hermle M, Dimroth F, Bett AW. Effects of optical coupling in III-V multilayer systems. *Applied Physics Letters* 2007; **90**: 192109. http://dx.doi.org/10.1063/1.2737927
17. Allen CR, Lim SH, Li JJ, Zhang YH. Simple method for determining luminescence coupling in multi-junction solar cells. *Proceedings of the 37th IEEE Photovoltaic Specialists Conference (PVSC)* 2011; 452–453.
18. Lim SH, Li JJ, Steenbergen EH, Zhang YH. Luminescence coupling effects on multijunction solar cell external quantum efficiency measurement. *Progress in Photovoltaics: Research and Applications* 2013; **21**: 344–350. DOI:10.1002/pip.1215.
19. Steiner MA, Kurtz SR, Geisz JF, McMahon WE, Olson JM. Using phase effects to understand measurements of the quantum efficiency and related luminescent coupling in a multijunction solar cell. *IEEE Journal of Photovoltaics* 2012; **2**: 424–433. DOI:10.1109/JPHOTOV.2012.2206566.
20. Steiner MA, Geisz JF. Non-linear luminescent coupling in series-connected multijunction solar cells. *Applied Physics Letters* 2012; **100**: 251106. DOI:10.1063/1.4729827.
21. Derkacs D, Bilir DT, Sabnis VA. Luminescent coupling in GaAs/GaInNAsSb multijunction solar cells. *IEEE Journal of Photovoltaics* 2013; **3**: 520–527. DOI:10.1109/JPHOTOV.2012.2213579.
22. Friedman DJ, Geisz JF, Steiner MA. Analysis of multijunction solar cell current–voltage characteristics in the presence of luminescent coupling. *IEEE Journal of Photovoltaics* 2013; **4**: 1429–1436. DOI:10.1109/JPHOTOV.2013.2275189.
23. Steiner MA, Geisz JF, García I, Friedman DJ, Duda A, Olavarria WJ, Young M, Kuciauskas D, Kurtz SR. Effects of internal luminescence and internal optics on the Voc and Jsc of III-V solar cells. *IEEE Journal of Photovoltaics* 2013; **4**: 1437–1442. 10.1109/JPHOTOV.2013.2278666
24. Nesswetter H, Jost NR, Lugli P, Bett AW, Zimmermann CG. Determination of subcell I-V parameters by a pulsed suns-Voc method including optical coupling. *Applied Physics Letters* 2015; **106**: 023903. DOI:10.1063/1.4906237.
25. Würfel P. *Physik der Solarzelle*. : Spektrum Akademischer Verlag GmbH, 2000.
26. Lindholm FA, Fossum JG, Burgess EL. Application of the superposition principle to solar-cell analysis. *IEEE Transactions on Electron Devices* 1979; **ED-26**: 165–171.
27. Guter G, Bett AW. I-V characterization of tunnel diodes and multijunction solar cells. *IEEE Transactions on Electron Devices* 2006; **53**: 2216–2222.
28. Rau U. Superposition and reciprocity in the electroluminescence and photoluminescence of solar cells. *IEEE Journal of Photovoltaics* 2012; **2**: 169.
29. Rau U. Reciprocity relation between photovoltaic quantum efficiency and electroluminescent emission of solar cells. *Physical Review B* 2007; **76**: 085303.
30. Zimmermann CG. Utilizing lateral current spreading in multijunction solar cells: an alternative approach to detecting mechanical defects. *Journal of Applied Physics* 2006; **100**: 23714. http://dx.doi.org/10.1063/1.2216868
31. King RR, Law DC, Edmondson KM, Fetzer CM, Kinsey GS, Yoon H, Sherif RA, Karam NH. 40% efficient metamorphic GaInP GaInAs Ge multijunction solar cells. *Applied Physics Letters* 2007; **90**: 183516. 10.1063/1.2734507
32. Struge MD. Optical absorption of gallium arsenide between 0.6 and 2.75 eV. *Physical Review* 1962; **127**: 768.
33. LTSpice IV, "http://www.linear.com/designtools/software/," accessed on 30/04/2012.
34. Steiner MA, Geisz JF, Moriarty TE, France RM, McMahon WE, Olson JM, Kurtz FDJ. Measuring IV curves and subcell photocurrents in the presence of luminescent coupling. *IEEE Journal of Photovoltaics* 2013; **3**: 879–887. DOI:10.1109/JPHOTOV.2012.2228298.
35. Zhu L, Kim C, Yoshita M, Chen S, Sato S, Mochizuki T, Akiyama H, Kanemitsu Y. Impact of sub-cell internal luminescence yields on energy conversion efficiencies of tandem solar cells: a design principle. *Applied Physics Letters* 2014; **104**: 31118.